INTERNATIONAL JOURNAL OF INTEGRATED ENGINEERING
ISSN: 2229-838X e-ISSN: 2600-7916

IJIE

Vol. 16 No. 5 (2024) 71-87
https://publisher.uthm.edu.my/ojs/index.php/ijie

Numerical Investigation of Cross Ventilation Flow in A Gable Roof Building with Asymmetric Opening Positions

Rupam Deka[1,3]*, Kalyan Kumar Das[2], Dipankar Das[3]

[1] *Department of Energy Engineering, Assam Science and Technology University, Jalukbari, Guwahati, 781013, INDIA*
[2] *Department of Mechanical Engineering, Assam Engineering College, Jalukbari, Guwahati, 781013, INDIA*
[3] *Department of Mechanical Engineering, Dibrugarh University Rajabheta, Dibrugarh, 786004, INDIA*

*Corresponding Author: rupamdeka@dibru.ac.in
DOI: https://doi.org/10.30880/ijie.2024.16.05.007

Article Info

Received: 6 March 2024
Accepted: 23 May 2024
Available online: 1 August 2024

Keywords

Natural ventilation, greenhouse gas emission, computational fluid dynamics (CFD), gable roof building, wind loading

Abstract

Natural ventilation can be a suitable alternative to mechanical ventilation as it is cost-effective and environmentally friendly. Therefore, an effective design of the natural ventilation system is very crucial. In this work, an attempt has been made to investigate the impact of opening positions and roof pitch on the performance of wind-induced cross-ventilation in a gable roof building. Numerical simulations were carried out using the computational fluid dynamics (CFD) technique based on the steady Reynolds averaged Navier-Stokes equations (RANS) model. Six configurations with asymmetric openings on opposite facades were considered to evaluate the effect of opening positions. Further, for studying the influence of roof pitch on the flow properties, three roof pitches, viz. 3:10, 5:10 and 7.5:10 were considered. It is found that the configuration with a windward opening in the middle and a leeward opening at the bottom (Configuration D) has the highest flow rate. The configuration with a windward opening at the top and a leeward opening at the bottom (Configuration B) has the lowest flow rate. Furthermore, the investigation with different roof pitches reveals that buildings with lower roof pitches are more vulnerable to wind loading due to higher flow separation at the windward eave. The investigation concludes that the opening position and roof pitch significantly influences the indoor airflow characteristics thereby affecting the ventilation performance.

1. Introduction

Our planet is facing a grave threat from global warming. Its adverse impacts pose a significant challenge to the existence of man and animals. Mechanical ventilation systems are employed to maintain a comfortable indoor environment in buildings. These systems are also one of the sources of greenhouse gases. An adequately designed natural ventilation system can reduce the use of mechanical ventilation systems to a large extent, thereby reducing energy costs and greenhouse gas emissions. Natural ventilation also improves indoor air quality and helps to maintain a healthy indoor environment [1].

Natural ventilation can be achieved mainly by two mechanisms namely single-sided ventilation, where openings are located only in a single facade, and cross ventilation, where openings are located on two different facades. Various works have been done to investigate the performance of single-sided ventilation [2-6].

However, cross ventilation attracted more interest from the designers as well as the researchers as it facilitates more airflow through the occupying space [7]. The airflow characteristics in and around a building due to cross-ventilation have been investigated previously using experimental and computational fluid dynamics (CFD) techniques. Heiselberg et al. [8] experimentally investigated the airflow distribution in a cross-ventilated building. The study revealed that the air velocity inside the building, which is strongly related to the ventilation performance, is affected by the shape of the window, its location and size. Consequently, various window shapes such as square [9], rectangular- horizontally long [10] and vertically long [11] have been considered to investigate the impact of opening shape on cross-ventilation. Later, Derakhshan & Shaker [12] and Bazdidi-Tehrani et al. [13] found that as the height-to-width ratio of the openings increases, the cross-ventilation also increases, and further suggested that the ventilation rate can be increased by using a rectangular opening instead of a square opening for the same wall porosity. Wall porosity is the ratio of the size of the opening to the size of the wall on which it is located.

As mentioned above another important factor in cross-ventilation is the position of the openings. If the openings are located axially on the opposite walls then it is called symmetric opening positions in contrast if they are located diagonally then it is known as asymmetric opening positions. Karava et al. [14] and Moey et al. [15] attempted to investigate the impact of opening positions on cross ventilation where they considered both symmetric and asymmetric opening configurations. The findings revealed that the highest ventilation rate is obtained for the symmetric configuration when both the windward and leeward openings are located close to the roof. Moreover, the ventilation rate increases for the configurations with windward openings located near the roof. Meroney [16] in his work also considered both symmetric and asymmetric opening configurations to compare the performance of different RANS (Reynolds-Averaged Navier Stokes) based turbulence models and it noted that all the turbulence models considered in this work have been able to predict the flow characteristics around the building with reasonably good accuracy. The study also revealed that even though the external flow is sensitive to the different turbulence models, negligible variations have been observed in the case of internal flow. Although Zhang et al. [17] favoured for Large Eddy Simulations (LES) model over RANS however, the computational cost involved with LES remains a challenge [18]. Díaz-Calderón et al. [19] evaluated the ventilation performance for various building configurations with symmetric opening positions located at different heights from the ground. They found that the ventilation performance is enhanced when openings are located at mid-height or near the ground.

It is worth mentioning here that the opening size also plays a vital role in cross-ventilation and various studies have been conducted to understand the effect of opening size. Moey et al. [20] studied the effect of varying sizes of the leeward opening keeping the size of the windward opening fixed on the internal flow field in a cross-ventilated building. The results indicated that with the increase in the leeward opening size as compared to the size of the windward opening, the pressure inside the building model decreases and the ventilation rate increases. Kato et al. [21] opined that the Orifice equation provides less accurate results in estimating the airflow rate through openings. However, Seifert et al. [22] argued that the Orifice equation can estimate the airflow rate with a reasonably good accuracy for smaller openings with wall porosity of up to 10% but its accuracy lowers for openings with wall porosity more than 10%. All these works basically considered flat-roof buildings.

Apart from flat roofs, gable roof buildings are also widely used for residential and commercial purposes. This has captured the attention of the researchers in investigating the ventilation performance in gable roof buildings. Ginger & Letchford [23] investigated the internal and external pressure acting on a gable roof building having only a single opening on the windward facade. They found that the large positive internal pressure is strongly correlated to the high suction pressure at the edge of the windward roof. Later, Xing et al. [24] carried out an experimental study to evaluate the pressure distributions in and around a gable roof building with openings on the windward and side walls only. In addition, CFD analysis is performed by considering both RANS equations and LES to replicate the experimental outcomes. It is reported that, for perpendicular wind direction, RANS efficiently predicts the flow field. However, for oblique wind loading, the LES performs better than RANS. Then, Yi et al. [25] experimentally investigated the airflow features inside a naturally ventilated dairy barn. A pitched roof building model was selected for the study, with one ridge opening of fixed height and two sidewall openings of adjustable height. However, due to the limited number of measurement points, the study couldn't provide detailed information on the flow field around the building. Hayati et al. [26] experimentally investigated the natural ventilation in a gable roof building through doors. They reported that cross ventilation is a much more efficient way for natural ventilation than single-opening ventilation. Moreover, investigations related to wind flow behaviour in the vicinity of buildings having saw-tooth roofs is also reported in the literature [27, 28].

As the roof shape of a building significantly affects the ventilation performance [29] and gable roof structures are the most common, therefore, a detailed investigation of the cross-ventilation in gable roof buildings is of utmost importance. Furthermore, no studies on cross-ventilation in the past considered asymmetric openings in gable roof buildings. Hence, the present work aims to investigate the cross-ventilation due to asymmetric openings on opposite walls in the case of gable roof buildings. For this purpose, steady-state RANS simulations are performed on six sets of asymmetric opening configurations. Furthermore, three different

Int. Journal of Integrated Engineering Vol. 16 No. 5 (2024) p. 71-87

roof pitches are considered to analyse the effects of variation in roof pitches. The methodology of these simulations is discussed in the next section.

2. Methodology

The impact on ventilation due to different positions of openings in the opposite walls in gable roof buildings is considered in the current investigation. The governing equations involved for the present case are the 3D steady RANS equations and the k-ω SST turbulence model is employed for closure of the solution. The numerical simulations were carried out in commercial CFD software package ANSYS-FLUENT version 19. The computational domain, boundary conditions, solver settings, and validations are discussed in the following subsections.

2.1 Computational Domain

The gable roof building model considered for the present investigation is of length (L) 12 m, width (W) 6 m and height (H) 6 m with a pitch of 5:10 (Fig. 1(a)). The upstream and downstream length is considered as 3H and 15H, respectively. Further, the vertical height and lateral width are 5H as measured from the building roof and side walls, respectively (Fig. 1(b)). These dimensions are chosen based on the guidelines of Franke et al. [30] and Tominaga et al. [31]. Further, the upstream length was chosen as 3H instead of 5H, as suggested by Blocken et al. [32]. The resulting dimensions of the domain are 114 m x 66 m x 37.5 m (LxWxH).

A hybrid mesh was generated in the computational domain where tetrahedral elements were used near the building, hexahedral elements away from the building and near all the solid boundaries prism elements were used to capture the boundary layer developed, as shown in Fig.2. The reason for employing the hexahedral elements away from the building instead of the tetrahedral elements can be attributed to the fact that hexahedral elements have higher aspect ratio than tetrahedral elements and due to which the number of elements in the computational domain reduces. As a result, numerical simulations require less computational time to complete.

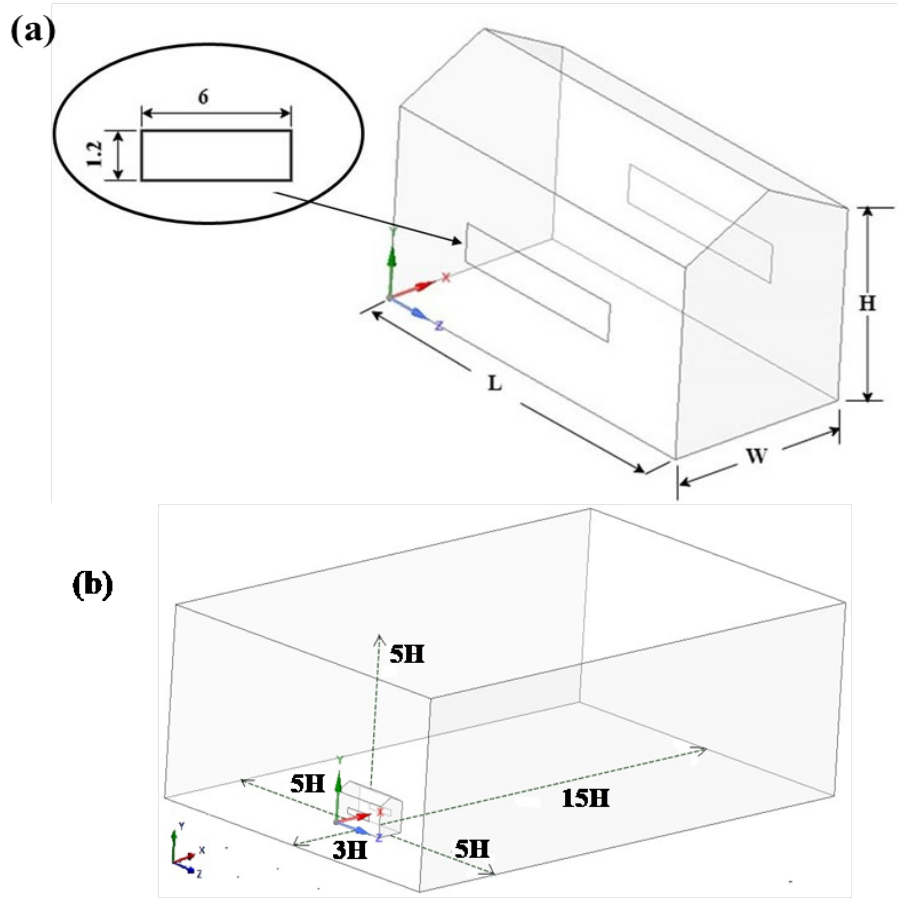

(All dimensions are in m)

Fig.1 *Perspective view of the (a) Building model; (b) Computational domain*

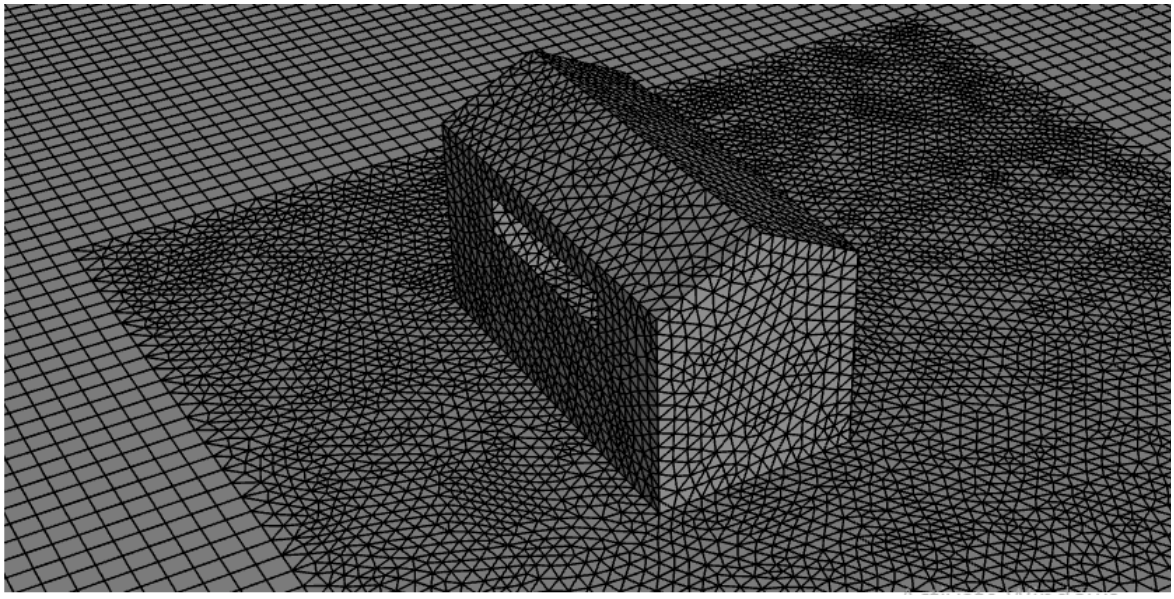

Fig. 2 *Perspective view of the computational grid*

2.2 Boundary Conditions

The inlet velocity was determined according to equation (1)

$$U(y) = \frac{u^*_{ABL}}{\kappa} \ln\left(\frac{y + y_o}{y_o}\right) \tag{1}$$

Where, u^*_{ABL} (=0.347 m/s) is the aerodynamic boundary layer (ABL) friction velocity, which is calculated from the reference velocity (U_{ref} =10 m/s) at eave height (y_{ref}=H=6 m) [33], κ is Von Karman constant (0.4), and y is the height coordinate and aerodynamic roughness length (y_o=0.0001 m). The turbulent kinetic energy can be calculated using equation (2)

$$k(y) = a\left(I_u(y).u(y)\right)^2 \tag{2}$$

Where the value of 'a' was selected as 1 (a=1) as recommended by Tominaga et al.[31] and the profile of streamwise turbulent intensity was chosen as per [34] as provided below

$$I_u(y) = \frac{1}{\ln\left(\frac{y}{y_o}\right)} \tag{3}$$

The turbulent dissipation rate is given by equation (4)

$$\varepsilon(y) = \frac{u^{*3}_{ABL}}{\kappa(y + y_o)} \tag{4}$$

The specific dissipation rate is defined in equation (5)

$$\omega(y) = \frac{\varepsilon(y)}{C_\mu k(y)} \tag{5}$$

Where the C_μ is an empirical constant taken as 0.09.

Int. Journal of Integrated Engineering Vol. 16 No. 5 (2024) p. 71-87

For the ground surface, the roughness constant C_s was assumed as 1, and the sand grain roughness height k_s could be determined using equation (6) according to their relationship with aerodynamic roughness length, y_o

$$k_s = \frac{9.793 y_o}{C_s} \tag{6}$$

For building surfaces, the roughness height and roughness constant were taken as 0 and 0.5. Symmetry boundary conditions were imposed on the sides and top of the domain with zero normal velocity and zero gradients for all variables. The outlet of the domain was imposed with zero static pressure.

2.3 Solver Settings

The present investigations involve the steady-state simulations of wind flow around 3-dimensional buildings. To accomplish the solution of the 3D steady RANS equations, the SIMPLE algorithm was used for pressure-velocity coupling. The pressure interpolation is of the second order, and all other transport equations are discretized by a second-order upwind scheme. Convergence is assumed to be obtained when all the scaled residuals levelled off reached a minimum of 10^{-5} for Continuity, x, y, Z momentum and k, and 10^{-4} for ω. It is important to note here that few simulations show oscillatory convergence. Therefore, the method of sampling and averaging, as suggested by [35], is employed in the present study. Where an additional criterion of streamwise wind speed (*U)* was monitored at three different locations, these locations are at the centre, upstream and downstream of the building. Simulations were carried out for 5000 iterations, and the results were sampled and averaged over the last 500 iterations.

2.4 Grid Sensitivity Test

A grid sensitivity test is performed on a configuration having symmetric opening positions where the centerline joining the windward and leeward opening is at a height of 3 m from the ground. This configuration is termed as reference case (Ref case) for the entire analysis and is shown in Fig. 3. Simulations were performed by considering the velocity profile mentioned in equation (1) with an aerodynamic boundary layer (ABL) friction velocity, u^*_{ABL} equal to 0.347 m/s for three different grids with 1721133 Cells (coarse grid), 2638635 cells (basic grid) and 4193546 cells (fine grid). The wind speed ratio (U/U_{ref}) obtained along the line joining the midpoint of the windward and leeward opening for all three grids are compared in Fig. 4. Here, a significant difference between the coarse and basic grid can be noticed. However, a further increase in the grid size doesn't alter the outcomes. Hence, the grid with 2638635 cells is chosen for the rest of the studies.

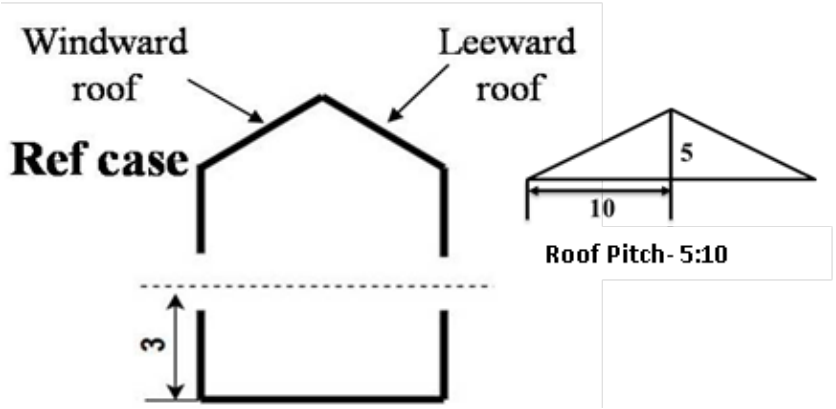

Fig. 3 *Schematic diagram of the reference case (Ref case) considered for the grid sensitivity test*

2.5 Validation

For validation purpose, CFD simulations are carried out to reproduce the experimental results of Karava et al. [14]. Here, the configuration with openings at the middle height and 10% wall porosity on both the windward and leeward walls is considered. A reference mean wind speed U_{ref} =6.97 m/s and a streamwise turbulence intensity of 10% at building height (H=80 mm) is considered. The streamwise and reference wind speed ratio (U/U_{ref}) obtained along a horizontal line joining the midpoint of windward, and the leeward opening is plotted and compared with the experimental results of [14] and the numerical results of Ramponi and Blocken [35] in Fig.5. A good agreement was observed between the present CFD work and the works of [35]. However, the

current CFD work showed minor deviations from the experimental results especially near the openings. Similar deviation is also reported by Ramponi and Blocken [35] and they are of the view that this is due to the effects of shadow and reflections. Moreover, the sharp variation in the wind speed in these regions also increases the uncertainties of PIV measurements.

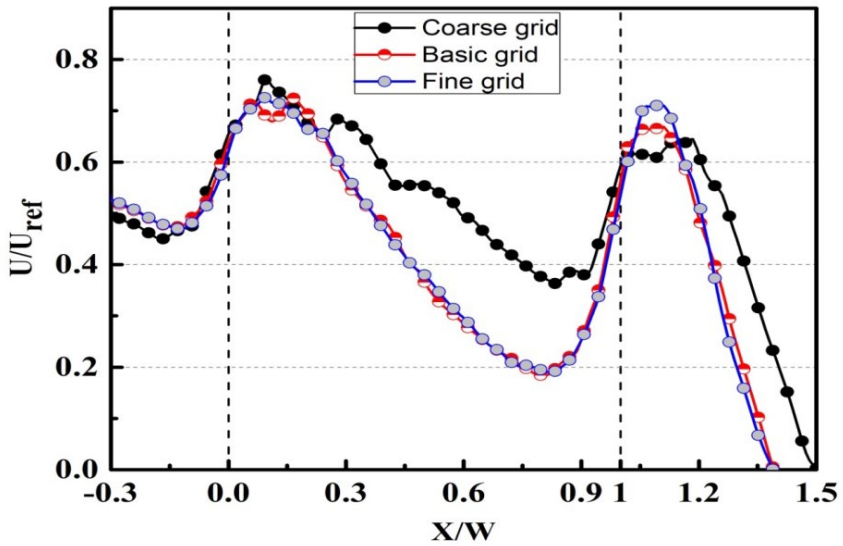

Fig. 4 *Comparison of non-dimensional streamwise wind velocity ratio for different grid resolutions*

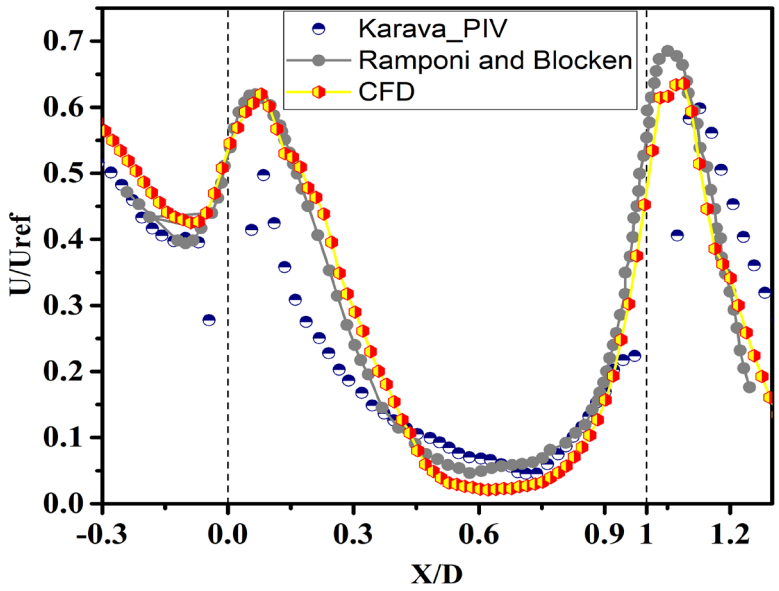

Fig. 5 *Comparison of non-dimensional streamwise wind velocity along the horizontal mid-line joining inlet and outlet opening*

3. Results and Discussion

3.1 Impact of Relative Opening Positions

The present study involves six different configurations namely A, B, C, D, E, and F based on the location of the openings at the windward and leeward walls. The positions of these openings are mentioned in Fig. 6. Furthermore, for all cases, the roof pitch is 5:10, and openings are of dimension 6 m x 1.2 m. In addition, the reference case (Ref case) is also taken into account for comparison purposes.

Int. Journal of Integrated Engineering Vol. 16 No. 5 (2024) p. 71-87

Simulations were performed using the same inlet parameters and grid size for configurations A, B, C, D, E and F. The velocity vector field obtained on the vertical mid-plane is shown in Fig. 7. The outside flow field is characterized by a standing vortex upstream of the building, separation of flow near the windward eaves and wake region downstream of the building. The standing vortex upstream of the building is found to be absent in configurations E and F, having windward openings below the mid-height. The main feature of the airflow inside the building is that a jet is formed as the air enters through the windward opening. In configurations C, D, E and F having the windward openings at or below the mid-height, the jet is directed downwards as it enters the building. This is due to the upstream recirculating flow and position of the windward opening [14]. However, for configurations A and B with the windward opening above the mid-height, the jet is directed upward (Fig. 8). Here, the area of positive pressure below the windward opening is higher than the area above the opening (Fig. 8). Therefore, the higher positive pressure below the inlet opening forces the air entering the building to move upward. Moreover, due to the flow separation occurring at the windward top corner, the air negotiates the corner, and the flow tries to move along the windward roof, resulting in an upward flow. This upward flow also influences the air flowing near the windward roof corner of the building and hence the air entering the buildings through the opening located above the mid-height forms an upward-moving jet (Fig. 8).

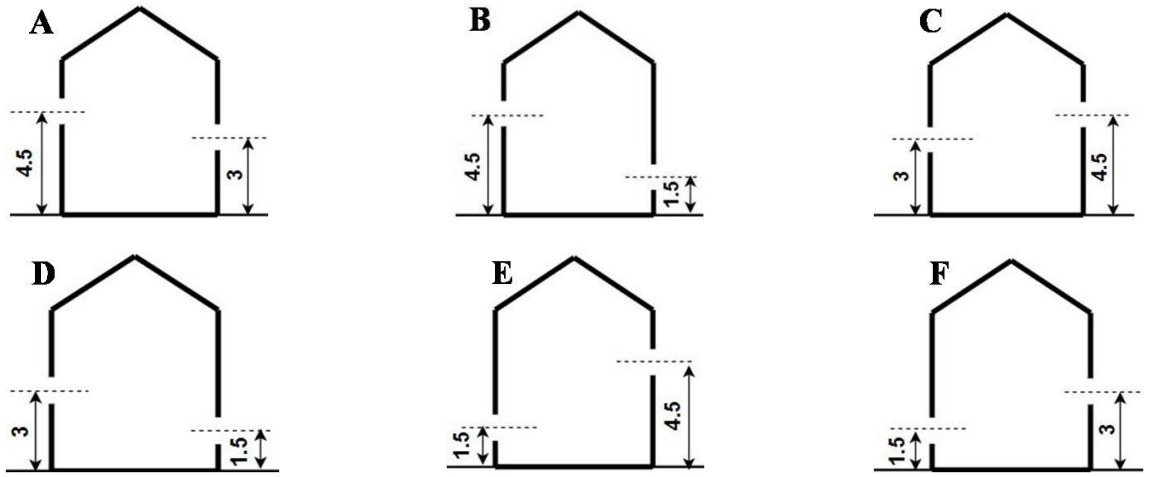

Fig. 6 *Schematic diagram of different configurations showing the position of windward and leeward openings*

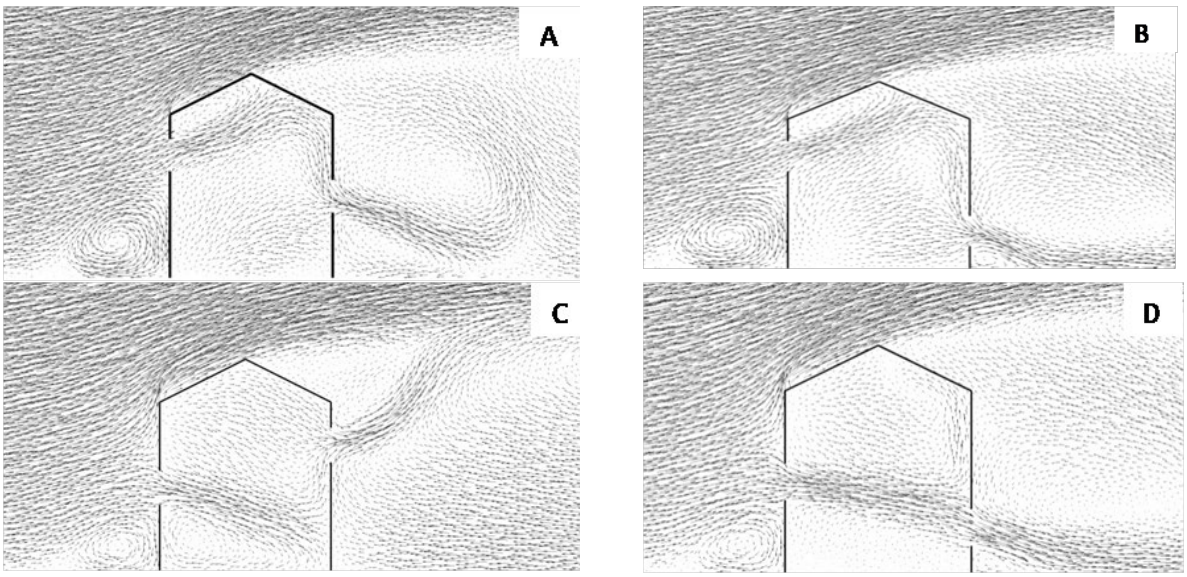

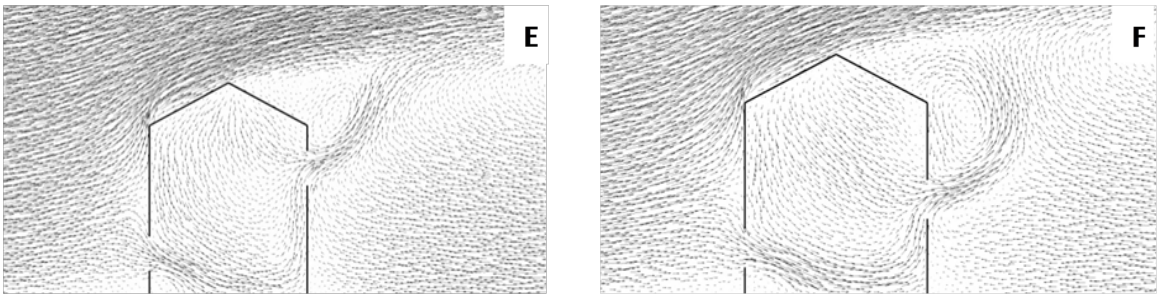

Fig. 7 *Velocity vector field obtained on vertical mid-plane for different configurations with roof pitch 5:10*

Furthermore, it is observed that the jet formed between the two openings first accelerates as it enters through the windward side since a vena-contract region is formed at the opening. This is consistent with Bernoulli's Law. For detailed analysis, the velocity along the horizontal centerline of windward openings in a streamwise direction is plotted in Fig. 9. Here, the maximum velocity attained for different configurations is noted to be at the non-dimensional distance of 0.04 to 0.146 as measured from the windward facade location. This is equal to 0.2-0.73 times the opening height. Moreover, the ratio of maximum velocity to the velocity at the windward opening ranges from 1.06 to 1.22. Here, the highest value is observed for configuration D. Nevertheless, after attaining the maximum velocity, the flow sharply decelerates as it passes through the central region.

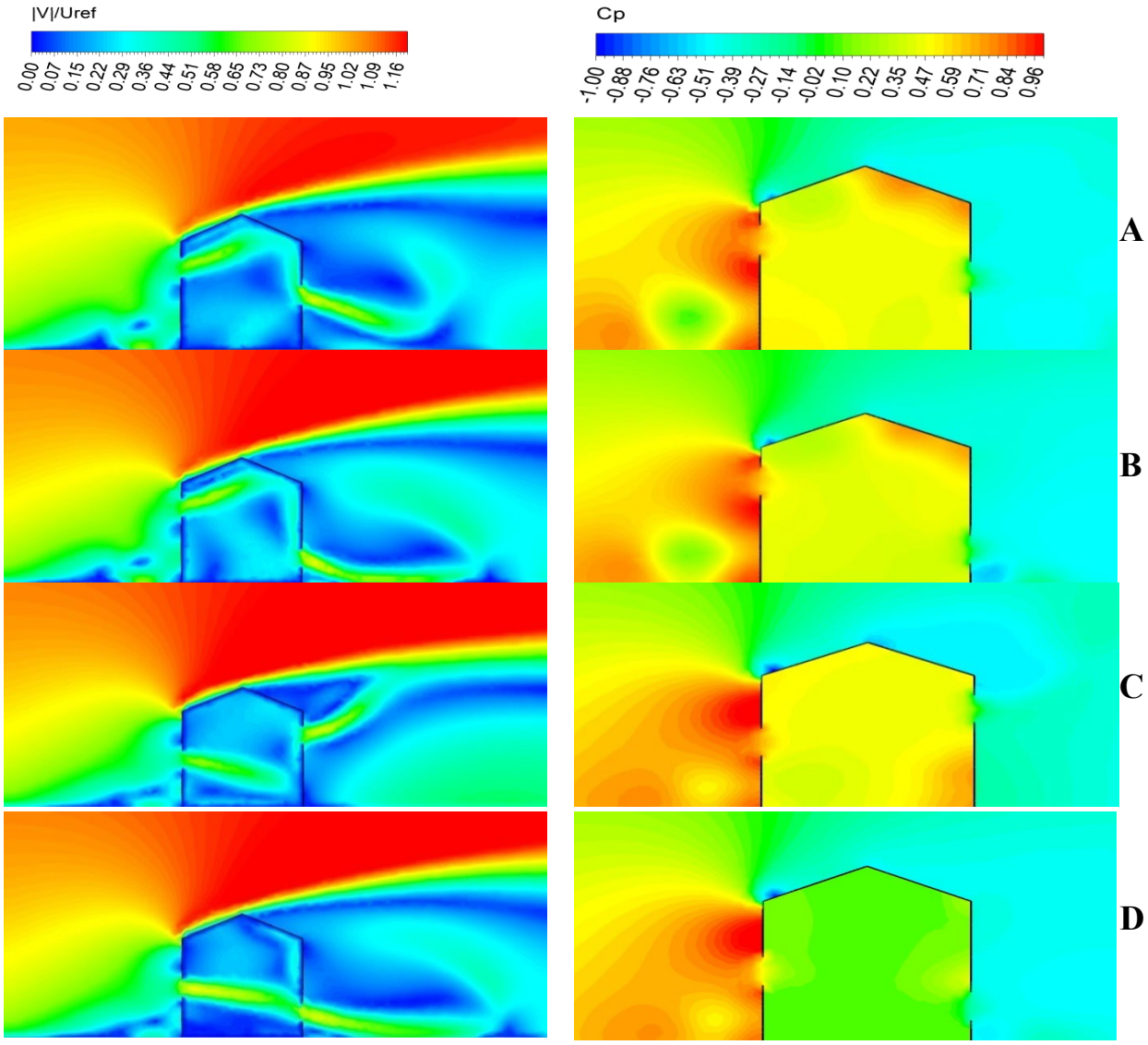

Int. Journal of Integrated Engineering Vol. 16 No. 5 (2024) p. 71-87

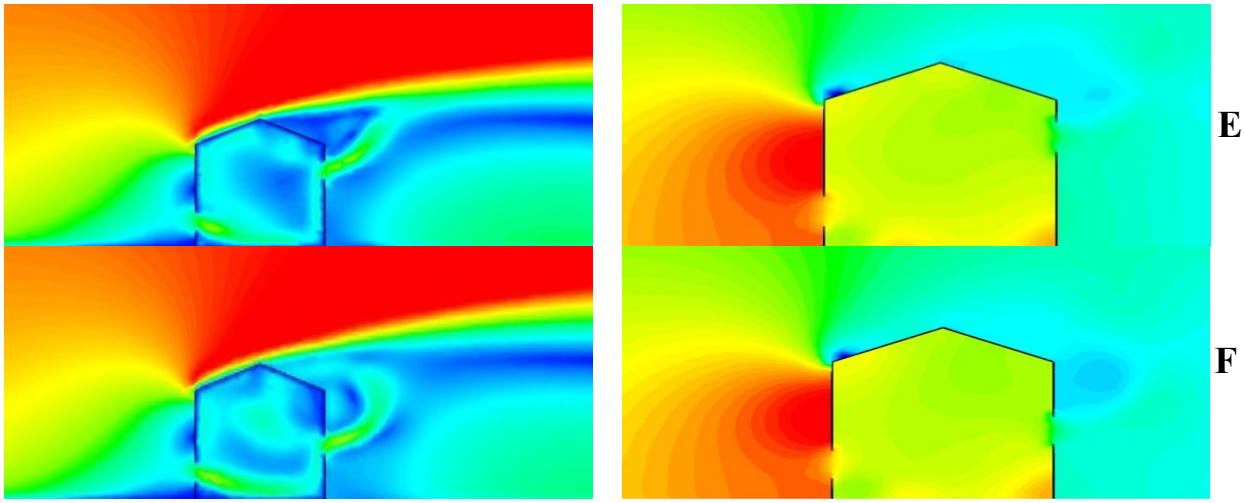

Fig. 8 *Contours of the non-dimensional velocity magnitude ($|V|/U_{ref}$) and coefficient of pressure (Cp) along the vertical mid-plane*

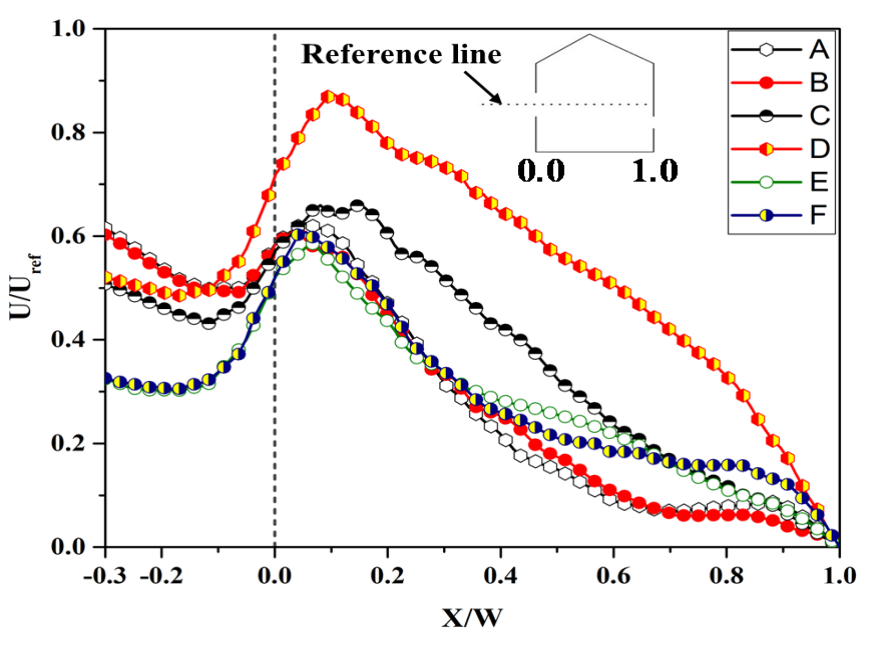

Fig. 9 *Non-dimensional streamwise wind speed (U/U_{ref}) along the horizontal centreline through the windward openings for various building configurations*

The volume flow rates through different configurations were evaluated to investigate the impact of the locations of the inlet and outlet openings. The volume flow rate obtained for all the configurations is shown in Fig. 10. It can be seen that for all cases except configuration D, the volume flow rate is less than the reference case. In configuration D, it is noted to be 10.11% higher. This can be explained by the mean internal pressure coefficient (Cp_{in}) variation shown in Fig. 11. Here, the mean internal pressure coefficient was estimated by taking the volume average of the coefficient of pressure (*Cp*) inside the building. It can be observed that Cp_{in} for configuration D is the minimum and hence, the jet experiences lower resistance leading to higher jet velocity. This in turn results in a higher flow rate.

3.2 Impact of Roof Pitch on The Cross-Ventilation Flow

The study continued to investigate the impact of roof pitch on flow behaviour inside and outside the gable roof buildings. For this purpose, three different gable roof configurations having roof pitches 3:10, 5:10 and 7.5: 10 were considered, as shown in Fig. 12. Simulations were performed for all the configurations mentioned in section 3.1 by considering these roof pitches. The pressure contours along the vertical mid-plane shown in Fig.

13 indicate that as the roof pitch increases from 3:10 to 7.5:10, the areas of positive pressure in front of the building increase. This rise is attributed to the enhancement in obstruction with the increase in roof pitch. Furthermore, for all the configurations with the lowest roof pitch (3:10), significant negative pressure regions are observed at the windward roof corners because of flow separation at this point. This negative pressure region tends to diminish with an increase in roof pitch as it weakens the flow separation.

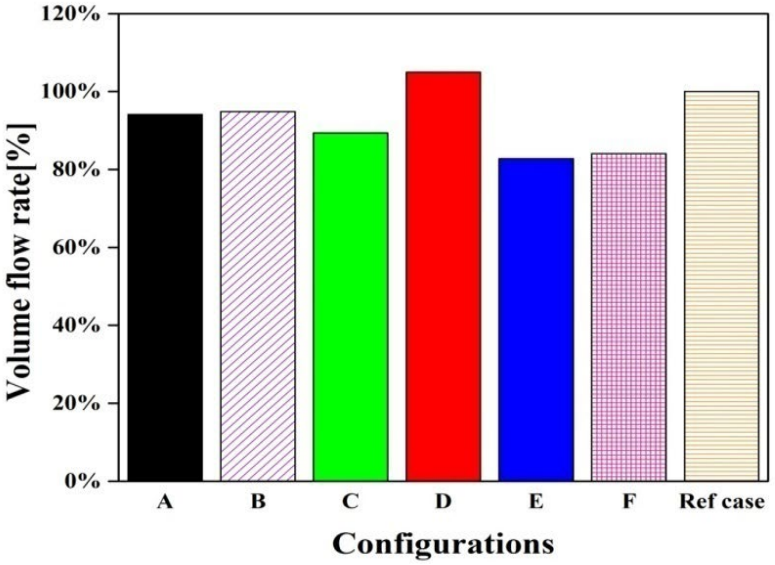

Fig. 10 *Volume flow rate for various configurations with roof pitch 5:10*

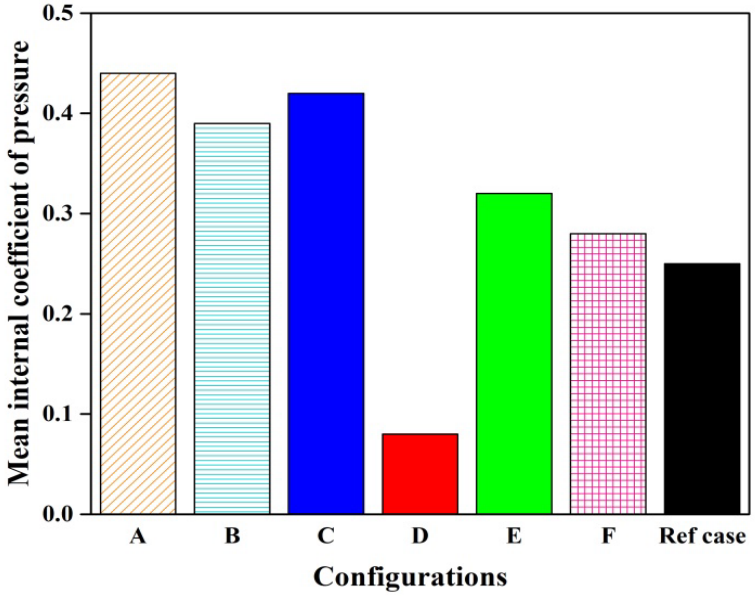

Fig. 11 *Mean internal coefficient of pressure for various configurations with roof pitch 5:10*

Int. Journal of Integrated Engineering Vol. 16 No. 5 (2024) p. 71-87

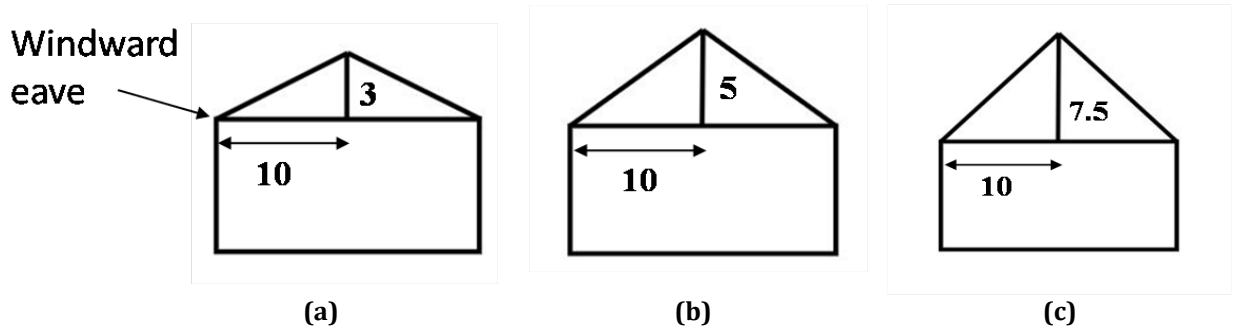

Fig. 12 *Schematic diagram of buildings with roof pitches (a) 3:10; (b) 5:10; (c) 7.5:10*

The volume flow rates obtained from the same set of simulations are compared in Fig. 14. It is observed that the volume flow rate increases with the increase in roof pitch except for configuration D. For this configuration, the maximum volume flow rate is obtained for the 5:10 roof pitch. This can be justified by the mean internal pressure coefficient variation shown in Fig. 15. Here, the least mean internal pressure coefficient is noted for the 5:10 pitch. This leads to comparatively lesser flow resistance resulting in a higher flow rate. Besides investigating the impact of roof pitch for all the asymmetric opening configurations (A-F), in Fig. 14(g) the volume flow rate for symmetric configurations with roof pitch 3:10 and 7.5:10 are compared with Ref case (i.e. symmetric configuration with 5:10 roof pitch). The variation of volume flow rate with roof pitch through buildings with symmetric opening configurations is similar to the asymmetric opening configurations. It is important to note that, the highest volume flow rate is obtained for configuration D irrespective of the roof pitch. Further, as compared to symmetric opening configurations, the volume flow rate for configuration D is found to be higher by 16.14%, 10.11% and 5% for roof pitches 3:10, 5:10 and 7.5:10 respectively.

Furthermore, the area-averaged coefficient of pressure (C_{pA}) on the windward roof for various configurations at different roof pitches is listed in Table 1. It is noted that for all the configurations, the C_{pA} values decrease very sharply with the decrease in roof pitch. Since the flow separation is more prominent in buildings with low roof pitch therefore very high negative values of C_{pA} were obtained for all the configurations with 3:10 roof pitch. Hence, the windward roof of the buildings with a 3:10 roof pitch is more vulnerable to wind loading. Further, it was observed that the roof pitch has little impact on the C_{pA} values on the leeward roof.

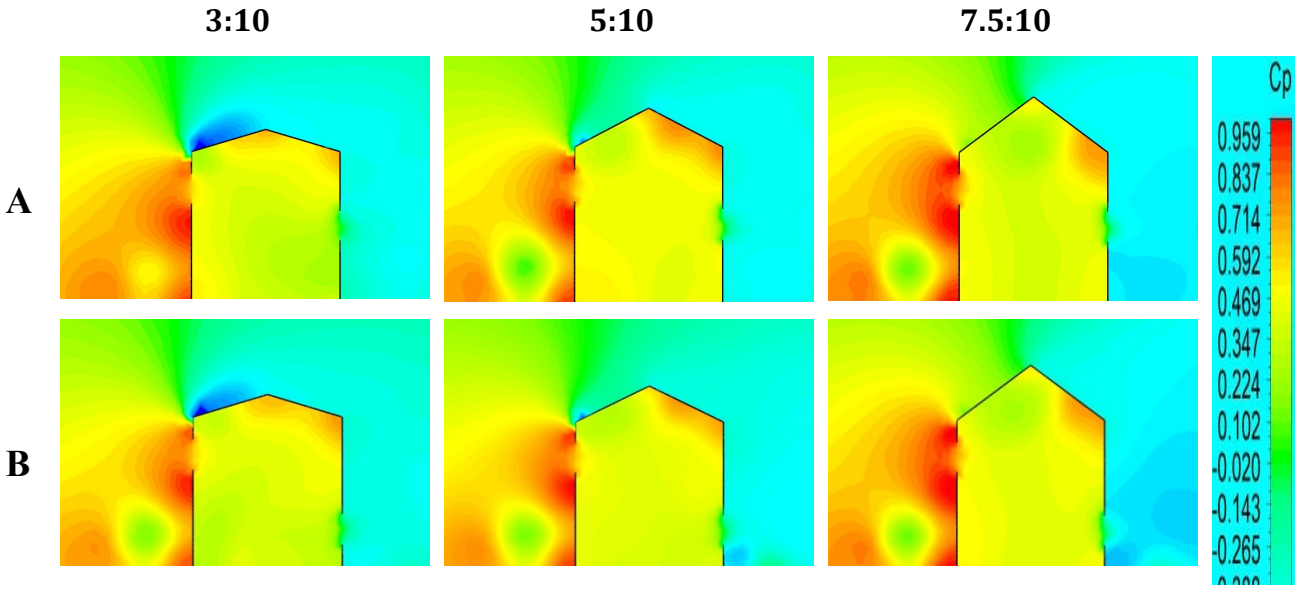

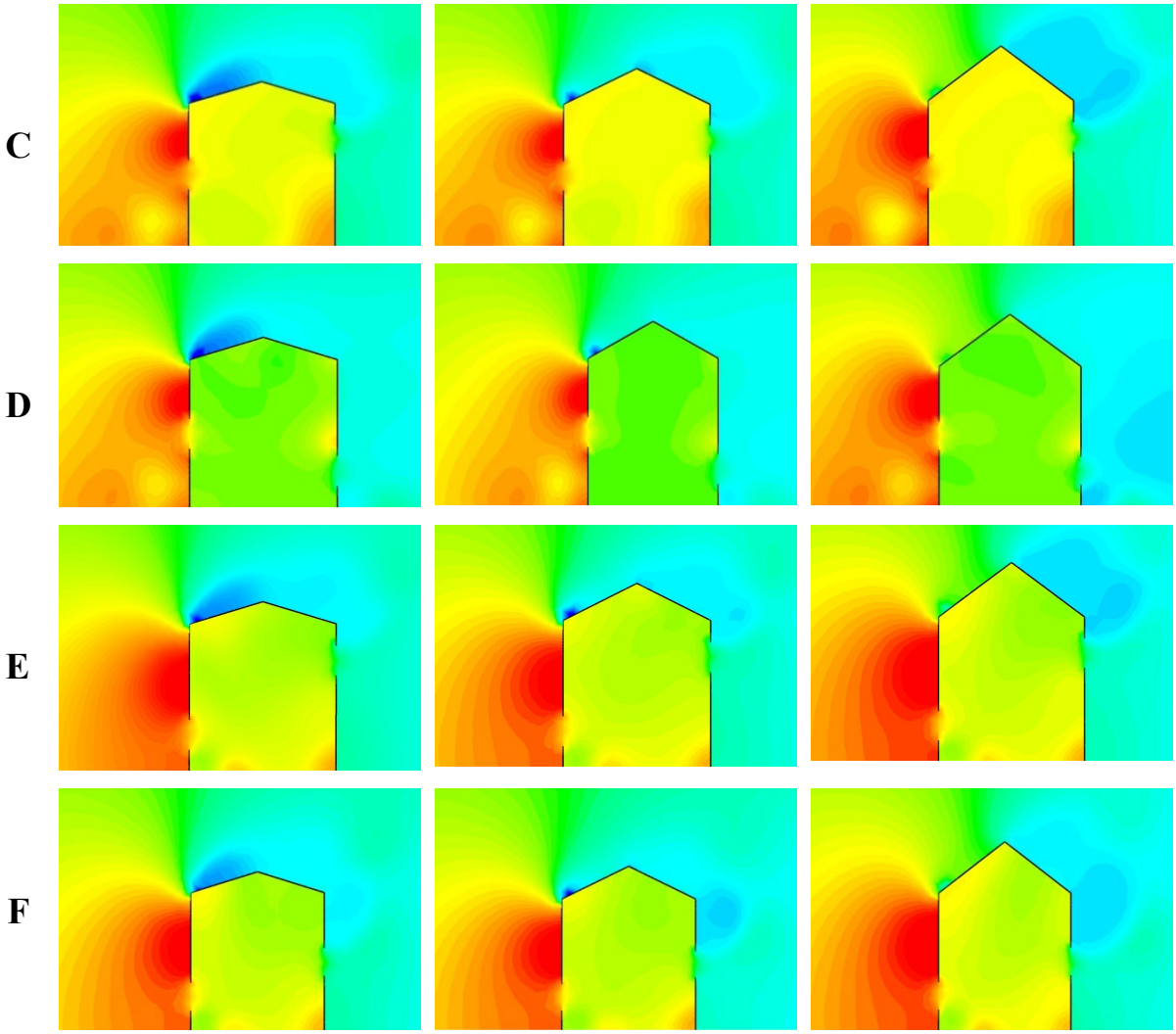

Fig. 13 *Coefficient of pressure contour on vertical mid-plane for building with various opening configurations and roof pitches*

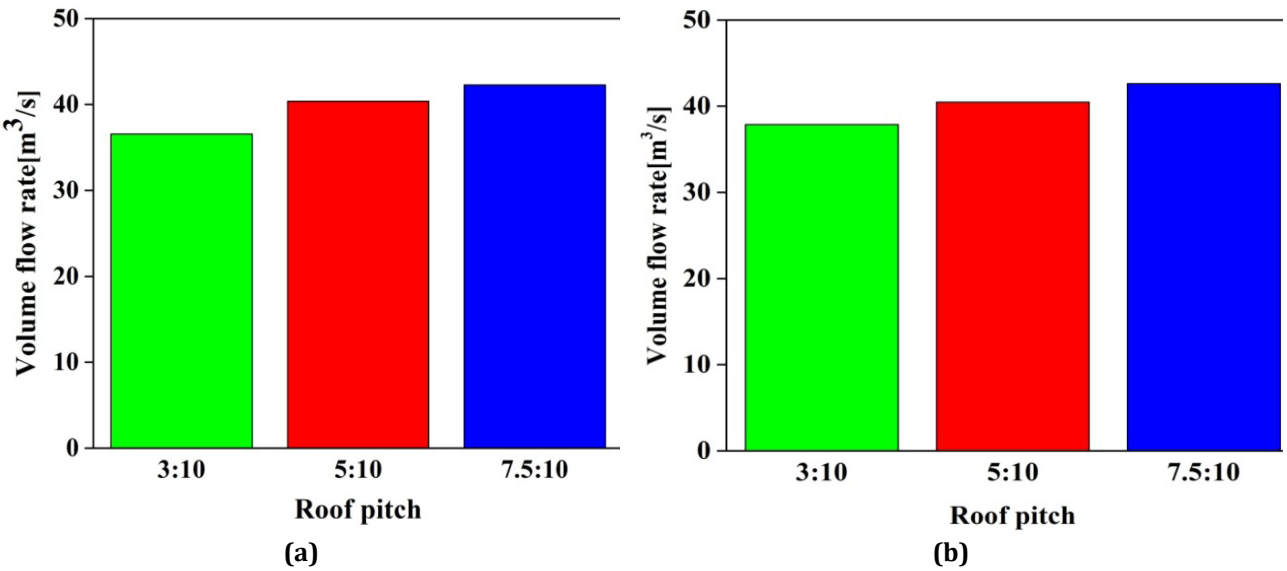

Int. Journal of Integrated Engineering Vol. 16 No. 5 (2024) p. 71-87

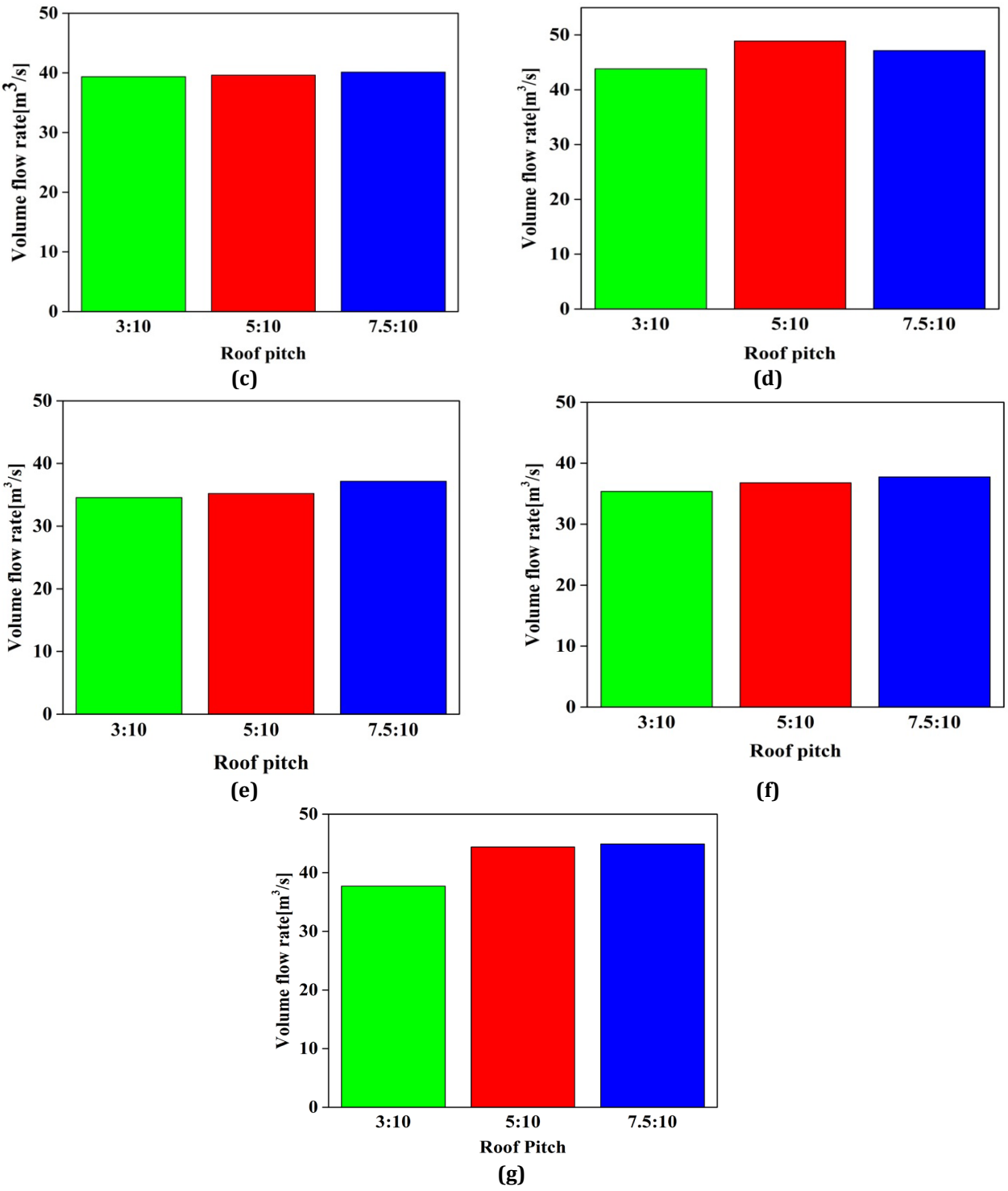

Fig. 14 *Volume flow rate obtained at different roof pitches for configuration (a) A; (b) B; (c) C; (d) D; (e) E; (f) F; (g) Ref case*

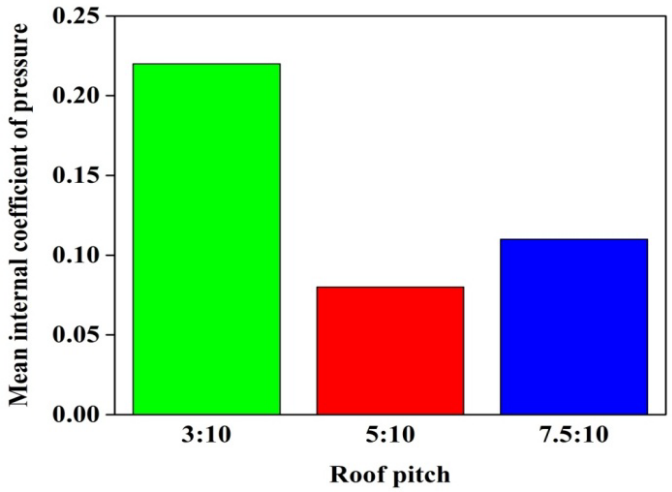

Fig. 15 *Mean internal coefficient of pressure obtained with various roof pitches for configuration D*

Table 1 *Area averaged coefficient of pressure on windward roofs obtained with different roof pitches for various configurations*

Configuration	Roof Pitch		
	3:10	5:10	7.5:10
A	-0.8453	-0.41	0.05
B	-0.8105	-0.4048	0.0643
C	-0.8483	-0.5328	-0.59
D	-0.8189	-0.49	-0.0007
E	-0.7985	-0.5736	-0.0667
F	-0.7652	-0.5471	-0.0495

4. Conclusion

In this work, numerical simulations were carried out to investigate the effect of variation in the location of openings and roof pitches on the cross-ventilation flow in and around the gable roof building. It is observed that the position of the windward opening significantly influences the indoor flow features. A jet is formed as the air passes through the windward opening. It moves downward for cases with a windward opening at or below the mid-height of the building, whereas it moves upward for cases with a windward opening above mid-height. This observation is true irrespective of the position of leeward openings. Furthermore, the jet initially accelerates as it enters through the windward opening up to a distance and then decelerates. The ratio of maximum velocity to the velocity at the inlet opening ranges from 1.06 to 1.22. The highest value of this ratio is achieved for configuration D, where the windward opening is located in the middle, and the leeward opening is located at the bottom. The lowest value is achieved for configuration B, where the windward opening is located at the top and the leeward opening is located at the bottom. Furthermore, the volume flow rate is found to be the highest for configuration D. This is because; the flow experiences the lowest resistance for this case due to the least mean internal pressure coefficient. The roof pitch has an appreciable impact on the pressure field surrounding the buildings for all configurations. With the increase in roof pitch, the area of positive pressure in front of the building increases as the blockage increases. The volume flow rate usually increases with the roof pitch; however, for configuration D, the maximum volume rate is obtained for the building with a roof pitch of 5:10. Another important observation is that for all the configurations with a roof pitch of 3:10, the area averaged coefficient of pressure on the windward roof of buildings is highly negative compared to the other two roof pitches. Therefore, it can be concluded that for lower roof pitches such as 3:10, the windward roof of the buildings is more susceptible to wind loading. In order to get a better insight into the cross-ventilation flow in gable roof buildings with asymmetric openings future research can take into account different wind incidence angles and wall porosities.

Acknowledgement

The authors express their gratitude to the Department of Mechanical Engineering, Dibrugarh University for permitting them to use the computational facility in the department.

Conflict of Interest

The authors declare that there is no conflict of interest.

Author Contribution

The authors confirm contribution to the paper as follows: ***Simulation, analysis and interpretation of results, draft manuscript preparation****: R Deka****; research plan, supervision the project****, and* ***revision the manuscript****: K K Das;* ***analysis and interpretation of results and revision the manuscript****: D Das. All authors reviewed the results and approved the final version of the manuscript.*

Funding

No financial assistance received for the project.

References

[1] Ohba, M., & Lun, I. (2010). Advances in Building Energy Overview of natural cross-ventilation studies and the latest simulation design tools used in building ventilation-related. *Advances in Building Energy Research*, *4*(1), 127–166.

[2] Cockroft, J. P., & Robertson, P. (1976). Ventilation of an enclosure through a single opening. *Building and Environment*, 11(1), 29–35. https://doi.org/10.1016/0360-1323(76)90016-0

[3] Dascalaki, E., Santamouris, M., Argiriou, A., Helmis, C., Asimakopoulos, D. N., Papadopoulos, K., & Soilemes, A. (1996). On the combination of air velocity and flow measurements in single sided natural ventilation configurations. *Energy and Buildings*, 24(2), 155–165. https://doi.org/10.1016/0378-7788(96)00973-5

[4] Kato, S., Kono, R., Hasama, T., Ooka, R., & Takahashi, T. (2006). A wind tunnel experimental analysis of the ventilation characteristics of a room with single-sided opening in uniform flow. *International Journal of Ventilation*, 5(1), 171–178. https://doi.org/10.1080/14733315.2006.11683734

[5] Larsen, T. S., & Heiselberg, P. (2008). Single-sided natural ventilation driven by wind pressure and temperature difference. *Energy and Buildings*, 40(6), 1031–1040. https://doi.org/10.1016/j.enbuild.2006.07.012

[6] Wang, H., & Chen, Q. (2012). A new empirical model for predicting single-sided, wind-driven natural ventilation in buildings. *Energy and Buildings*, 54, 386–394. https://doi.org/10.1016/j.enbuild.2012.07.028

[7] Jiang, Y., Alexander, D., Jenkins, H., Arthur, R., & Chen, Q. (2003). Natural ventilation in buildings: Measurement in a wind tunnel and numerical simulation with large-eddy simulation. *Journal of Wind Engineering and Industrial Aerodynamics*, 91(3), 331–353. https://doi.org/10.1016/S0167-6105(02)00380-X

[8] Heiselberg, P., Svidt, K., & Nielsen, P. V. (2001). Characteristics of airflow from open windows. *Building and Environment*, 36(7), 859–869. https://doi.org/10.1016/S0360-1323(01)00012-9

[9] Chu, C. R., Chiu, Y. H., Tsai, Y. T., & Wu, S. L. (2015). Wind-driven natural ventilation for buildings with two openings on the same external wall. *Energy and Buildings*, 108, 365–372. https://doi.org/10.1016/j.enbuild.2015.09.041

[10] Tominaga, Y., & Blocken, B. (2016). Wind tunnel analysis of flow and dispersion in cross-ventilated isolated buildings: Impact of opening positions. *Journal of Wind Engineering and Industrial Aerodynamics*, 155, 74–88. https://doi.org/10.1016/j.jweia.2016.05.007

[11] Manolesos, M., Gao, Z., & Bouris, D. (2018). Experimental investigation of the atmospheric boundary layer flow past a building model with openings. *Building and Environment*, 141(May), 166–181. https://doi.org/10.1016/j.buildenv.2018.05.049

[12] Derakhshan, S., & Shaker, A. (2016). Numerical study of the cross-ventilation of an isolated building with different opening aspect ratios and locations for various wind directions. *International Journal of Ventilation*, 16:1, 42-60. https://doi.org/10.1080/14733315.2016.1252146

[13] Bazdidi-Tehrani, F., Masoumi-Verki, S., & Gholamalipour, P. (2020). Impact of opening shape on airflow and pollutant dispersion in a wind-driven cross-ventilated model building: Large eddy simulation. *Sustainable Cities and Society*, *61*, 102196. https://doi.org/10.1016/j.scs.2020.102196

[14] Karava, P., Stathopoulos, T., & Athienitis, A. K. (2011). Airflow assessment in cross-ventilated buildings with operable façade elements. *Building and Environment*, *46*(1), 266–279. https://doi.org/10.1016/j.buildenv.2010.07.022

[15] Moey, L. K., Chan, K. L., Tai, V. C., Go, T. F., & Chong, P. L. (2021). Investigation on the effect of opening position across an isolated building for wind-driven cross ventilation. *Journal of Mechanical Engineering and Sciences*, 15(2), 8141–8152. https://doi.org/10.15282/jmes.15.2.2021.14.0639
[16] Meroney, R. N. (2009). CFD Prediction of Airflow in Buildings for Natural Ventilation. 11th Americas Conference on Wind Engineering, Puerto Rico.
[17] Zhang, X., Weerasuriya, A. U., and Tse, K. T. (2020). CFD Simulation of Natural Ventilation of a Generic Building in Various Incident Wind Directions : Comparison of Turbulence Modelling , Evaluation Methods , and Ventilation Mechanisms. *Energy and Buildings*, 229, 110516. https://doi.org/10.1016/j.enbuild.2020.110516
[18] Hwang, Y., and Gorlé, C. (2022). Large-Eddy Simulations of Wind-Driven Cross Ventilation, Part1: Validation and Sensitivity Study, *Frontiers in Built Environment*, 8, 1–34.
[19] Díaz-Calderón, S. F., Castillo, J. A., and Huelsz, G. (2023). Evaluation of different window heights and facade porosities in naturally cross-ventilated buildings: CFD validation. *Journal of Wind Engineering and Industrial Aerodynamics*, 232, 105263.
[20] Moey, L. K., Sing, Y. H., Tai, V. C., Go, T. F., and Sia, Y. Y. (2021). Effect Of Opening Size On Wind- Driven Cross Ventilation. *International Journal of Integrated Engineering*, 13(6), 99–108.
[21] Kato, S., Murakami, S., Mochida, A., Akabayashi, S. ichi, & Tominaga, Y. (1992). Velocity-pressure field of cross ventilation with open windows analyzed by wind tunnel and numerical simulation. *Journal of Wind Engineering and Industrial Aerodynamics*, 44(1–3), 2575–2586. https://doi.org/10.1016/0167-6105(92)90049-G
[22] Seifert, J., Li, Y., Axley, J., & Rösler, M. (2006). Calculation of wind-driven cross ventilation in buildings with large openings. *Journal of Wind Engineering and Industrial Aerodynamics,* 94(12), 925–947. https://doi.org/10.1016/j.jweia.2006.04.002
[23] Ginger, J. D., & Letchford, C. W. (1999). Net pressures on a low-rise full-scale building. *Journal of Wind Engineering and Industrial Aerodynamics*, 83(1–3), 239–250. https://doi.org/10.1016/S0167-6105(99)00075-6
[24] Xing, F., Mohotti, D., & Chauhan, K. (2018). Study on localised wind pressure development in gable roof buildings having di ff erent roof pitches with experiments , RANS and LES simulation models. *Building and Environment*, 143(May), 240–257. https://doi.org/10.1016/j.buildenv.2018.07.026
[25] Yi, Q., König, M., Janke, D., Hempel, S., Zhang, G., Amon, B., & Amon, T. (2018). Wind tunnel investigations of sidewall opening effects on indoor airflows of a cross-ventilated dairy building. *Energy and Buildings*, 175, 163–172. https://doi.org/10.1016/j.enbuild.2018.07.026
[26] Hayati, A., Mattsson, M., & Sandberg, M. (2018). A wind tunnel study of wind-driven airing through open doors. *International Journal of Ventilation*, 18(2), 113–135. https://doi.org/10.1080/14733315.2018.1435027
[27] Perén, J. I., van Hooff, T., Leite, B. C. C., & Blocken, B. (2015). CFD analysis of cross-ventilation of a generic isolated building with asymmetric opening positions: Impact of roof angle and opening location. *Building and Environment*, 85, 263–276. https://doi.org/10.1016/j.buildenv.2014.12.007
[28] Perén, J. I., van Hooff, T., Leite, B. C. C., & Blocken, B. (2016). CFD simulation of wind-driven upward cross ventilation and its enhancement in long buildings: Impact of single-span versus double-span leeward sawtooth roof and opening ratio. *Building and Environment*, 96, 142–156. https://doi.org/10.1016/j.buildenv.2015.11.021
[29] Tominaga, Y., Akabayashi, S., Kitahara, T., and Arinami, Y. (2015). Air flow around isolated gable-roof buildings with different roof pitches: Wind tunnel experiments and CFD simulations. *Building and Environment*, 84, 204–213.
[30] Franke, J., Hellsten, A., Schlünzen, H., & Carissimo, B. (2007). Best Practice Guideline for the CFD Simulation of Flows in the Urban Environment. Brussels:COST Office.
[31] Tominaga, Y., Mochida, A., Yoshie, R., Kataoka, H., Nozu, T., Yoshikawa, M., & Shirasawa, T. (2008). AIJ guidelines for practical applications of CFD to pedestrian wind environment around buildings. *Journal of Wind Engineering and Industrial Aerodynamics*, 96(10–11), 1749–1761. https://doi.org/10.1016/j.jweia.2008.02.058
[32] Blocken, B., Stathopoulos, T., and Carmeliet, J. (2007). CFD simulation of the atmospheric boundary layer: wall function problems. *Atmospheric Environment*, 41(2), 238–252, 2007.
[33] Hargreaves D.M. and Wright N.G. (2006). The use of commercial CFD software to model the atmospheric boundary layer. The Fourth International Symposium on Computational Wind Engineering (CWE2006), Yokohama.
[34] Karava, P. (2008). Airflow Prediction in buildings for Natural Ventilation Design:wind tunnel measurements and simulation, Ph. D. Dissertation, Department of Building, Civil and Environmental Engineering, Concordia University, Montreal, Canada.

Int. Journal of Integrated Engineering Vol. 16 No. 5 (2024) p. 71-87

[35] Ramponi, R., & Blocken, B. (2012). CFD simulation of cross-ventilation flow for different isolated building configurations: Validation with wind tunnel measurements and analysis of physical and numerical diffusion effects. *Journal of Wind Engineering and Industrial Aerodynamics*, 104–106, 408–418. https://doi.org/10.1016/j.jweia.2012.02.005